Supplementary Materials

1. Yeast strains and plasmids

All strains used in this study are derivatives from YACL-379 (MATa *can1::HO-CAN1 ho::HO-ADE2 ura3 ade2 leu2 trp1 his3 bar1*) strain of W303a genetic background (1). Note that the BAR1 gene coding for α-factor specific protease has been deleted. The relevant genotypes of the different strains used in this study are shown in Table S1.

The number of YFP-STE5 integrations was estimated from the level of YFP fluorescence in unstimulated cells. The increase in fluorescence is quantal, meaning that the difference of mean fluorescence between two strains is an integer multiple of the minimum difference observed between strains. This quantal increase in fluorescence is consistent with the discrete number of integrations of the P_{STE5}-YFP-STE5 construct, and the fact that the STE5's promoter does not depend on the pheromone response and is insensitive to the level of Ste5 within the cell (2).

In Figure S1 we show a plot of the mean fluorescence level for strains with different number of integrations. Note that the strains are ordered on the x axis according to their level of

fluorescence. The excellent linear fit (R^2=0.995) demonstrates that the assigned integration number is consistent with the mean fluorescence level.

Strain	Relevant Genotype	#YFP-STE5
YACL379	(parental strain) (1)	0
RY2013b	ste5::YFP-STE5 trp1::P_{STE5}-YFP-STE5::TRP1 fus3::FUS3-Q93A::URA3 (3)	2
TCY3056	ste5::YFP-STE5 (2)	1
TCY3057	ste5::YFP-STE5 trp1::P_{STE5}-YFP-STE5::TRP1 (2)	2
TCY3073	bmh2::BMH2-YFP::HIS5	0
TCY3099	ste5::YFP-STE5, CFP-STE4	1
TCY3100	CFP-STE4	0
TCY3126	leu2::P_{PRM1}-CFP::LEU2, CDC28-F88A, ste5::YFP-STE5	1
TCY3127	leu2::P_{PRM1}-CFP::LEU2, CDC28-F88A, ste5::YFP-STE5 trp1::YFP-STE5::TRP1	2
TCY3205	leu2::P_{PRM1}-CFP::LEU2, CDC28-F88A, ste5::YFP-STE5 trp1::YFP-STE5::TRP1, ⊗ste4::kanMX6	2
YAB3759	leu2::P_{PRM1}-CFP::LEU2, CDC28-F88A, ste5::YFP-STE5, trp1::P_{STE5}-YFP-STE5::TRP1	2
YAB3760	leu2::P_{PRM1}-CFP::LEU2, CDC28-F88A, ste5::YFP-STE5, trp1::P_{STE5}-YFP-STE5::TRP1	2
YAB3761	leu2::P_{PRM1}-CFP::LEU2, CDC28-F88A, ste5::YFP-STE5, (trp1::P_{STE5}-YFP-STE5::TRP1)x3	4
YAB3762	leu2::P_{PRM1}-CFP::LEU2, CDC28-F88A, ste5::YFP-STE5, (trp1::P_{STE5}-YFP-STE5::TRP1)x5	6
YAB3764	leu2::P_{PRM1}-CFP::LEU2, CDC28-F88A, ste5::YFP-STE5, trp1::P_{STE5}-YFP-STE5::TRP1, ste5::P_{STE5}-YFP-STE5::URA3	3
YAB3765	leu2::P_{PRM1}-CFP::LEU2, CDC28-F88A, ste5::YFP-STE5, (trp1::P_{STE5}-YFP-STE5::TRP1, ste5::P_{STE5}-YFP-STE5::URA3)x3	4
YAB3766	leu2::PPRM1-CFP::LEU2, CDC28-F88A, ste5::YFP-STE5, (trp1:: P_{STE5}-YFP-STE5::TRP1, ste5::P_{STE5}-YFP-STE5::URA3)x6	7
YAB3767	leu2::PPRM1-CFP::LEU2, CDC28-F88A, ste5::YFP-STE5, (trp1:: P_{STE5}-YFP-STE5::TRP1, ste5::P_{STE5}-YFP-STE5::URA3)x5	6
YAB3770	leu2::PPRM1-CFP::LEU2, CDC28-F88A, ste5::YFP-STE5, (trp1::P_{STE5}-YFP-STE5::TRP1, ste5::P_{STE5}-YFP-STE5::URA3)x8	9
YAB3771	ste5::YFP-STE5, CFP-STE4, ste5::P_{STE5}-YFP-STE5::TRP1	2
YAB3772	CFP-STE4, ste5::YFP-STE5, ste5:: P_{STE5}-YFP-STE5::TRP1, ste5::P_{STE5}-YFP-STE5::URA3	3
YAB3773	CFP-STE4, ste5::YFP-STE5, ste5::P_{STE5}-YFP-STE5::TRP1, ste5::P_{STE5}-YFP-STE5::URA3	3
YAB3774	CFP-STE4, ste5::YFP-STE5, (ste5::P_{STE5}-YFP-STE5::TRP1, ste5::P_{STE5}-YFP-STE5::URA3)x3	4
YAB3775	CFP-STE4, ste5::YFP-STE5, (ste5::P_{STE5}-YFP-STE5::TRP1, ste5::P_{STE5}-YFP-STE5::URA3)x3	4
YAB3776	CFP-STE4, ste5::YFP-STE5, (ste5::P_{STE5}-YFP-STE5::TRP1, ste5::P_{STE5}-YFP-STE5::URA3)x4	5
YAB3777	CFP-STE4, ste5::YFP-STE5, (ste5::P_{STE5}-YFP-STE5::TRP1, ste5::P_{STE5}-YFP-STE5::URA3)x4	5

Table S1: Relevant genotypes of yeast strains used in this study. All strains are derivatives of YACL379 (MATa *Δbar1*) of W303a genetic background. Number of YFP-STE5 as assessed by fluorescence microscopy is shown

in the #YFP-STE5 column. The “(,)x3” notation means there are overall 3 copies of the constructs within the brackets, not three copies of each construct.

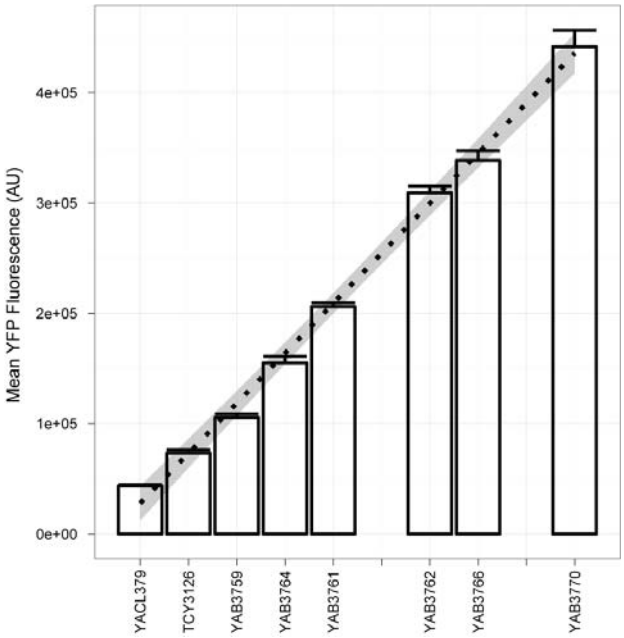

Figure S1: Mean YFP fluorescence for different strains ordered by integration number. Error bars represent the 95% confidence interval for the mean. The dashed line is the best linear fit for the fluorescence level versus estimated integration number (slope=45±1 10^3AU, intercept=28±6 10^3AU). The shaded region is the 95% confidence interval for this fit.

2. Numeric simulations of Cell-ID variables and candidate statistics

The boundaries for each cell are found by our software Cell-ID(2, 4) based of a purposely defocused bright field image. Based on these boundaries, the program defines several subcellular regions, and calculates the area and fluorescence for each channel within these regions. Particularly relevant for the measurement of membrane recruitment are the features measured on annular regions concentric to the cell´s boundary (Table S2 and Figure S2A).

To gain insight into the quantitative dependence of each of Cell-ID´s features with the fraction of membrane bound fluorescence, we created and analyzed simulated images. The intensity of each pixel of an image is the result of two factors; the fluorophore distribution within the sample and the optics of the microscope.

For simplicity we approximated the cell´s morphology by a sphere of 5µm of diameter, with the fluorophores homogeneously distributed in the sphere volume for the 0% recruitment simulation, or in the sphere surface for 100% recruitment. By combining these two extreme distributions any intermediate distribution can be simulated.

Feature	Description
f.tot	Sum of the fluorescence image for all the pixels found in that cell
a.tot	Area of the cell in pixels
maj.axis	Length of the major axis in pixel units
min.axis	Length of the minor in pixel units
f.local.bg	Mean background fluorescence per pixel, measured from pixels located 5 radial pixels further out than the cell boundary. Only pixels along the annular boundary NOT associated with ANY cell are included.
f.p1	Fluorescence integrated in the annular region that is one pixel outside the cell boundary
a.p1	Area of the the annular region that is one pixel outside the cell boundary
f.m0	Fluorescence integrated on the cell boundary
a.m0	Area of the cell boundary
f.m1	Fluorescence integrated in the annular region that is one pixel inwards from the cell boundary
a.m1	Area of the annular region that is one pixel inwards from the cell boundary
f.m2	Fluorescence integrated in the annular region that is two pixels inwards from the cell boundary
a.m2	Area of the annular region that is two pixels inwards from the cell boundary
f.tot.m3	Fluorescence of all pixels interior to the boundary that are three pixels or more away from the cell boundary
a.tot.m3	Area of all pixels interior to the boundary that are three pixels or more away from the cell boundary

Table S2: Description of features calculated by Cell-ID, used for the construction of the membrane recruitment statistic.

The optics of the microscope can be captured by its “Point Spread Function” (PSF),that describes how the light emitted from one point in the sample spreads on the detector, and reflects the diffraction limited resolution of optical systems. Equivalently, the PSF describes the probability with which a photon emitted from each point in the sample is detected. In this sense the PSF defines the focal volume. For a confocal microscope a common approximation is to consider the PSF as a 3D Gaussian (5).

$$PDF(x,y,z) \propto \exp\left(-\frac{x^2+y^2}{2\sigma_{xy}^2}\right)\exp\left(-\frac{z^2}{2\sigma_z^2}\right) \qquad \text{Equation S1}$$

The parameters σ_{xy} and σ_z represent the width of the PSF in the XY and Z directions, respectively. The full width at half maximum (FWHM) is given by 2.35σ.

The intensity of any given pixel ($F_{i,j}$) is proportional to the convolution between the sample fluorophore distribution C(x,y,z) and the PSF centered at the position correspondent to that pixel.

$$F_{i,j} \propto \iiint_{Sample} PSF(x-x_0, y-y_0, z-z_0)\, C(x,y,z)\, dx\, dy\, dz$$

Equation S2

In this way we could create simulated fluorescence images for different fluorescence distributions, and calculate Cell-ID´s features on these simulated images. The simulations were done in Mathematica 5.0 (Wolfram Research).

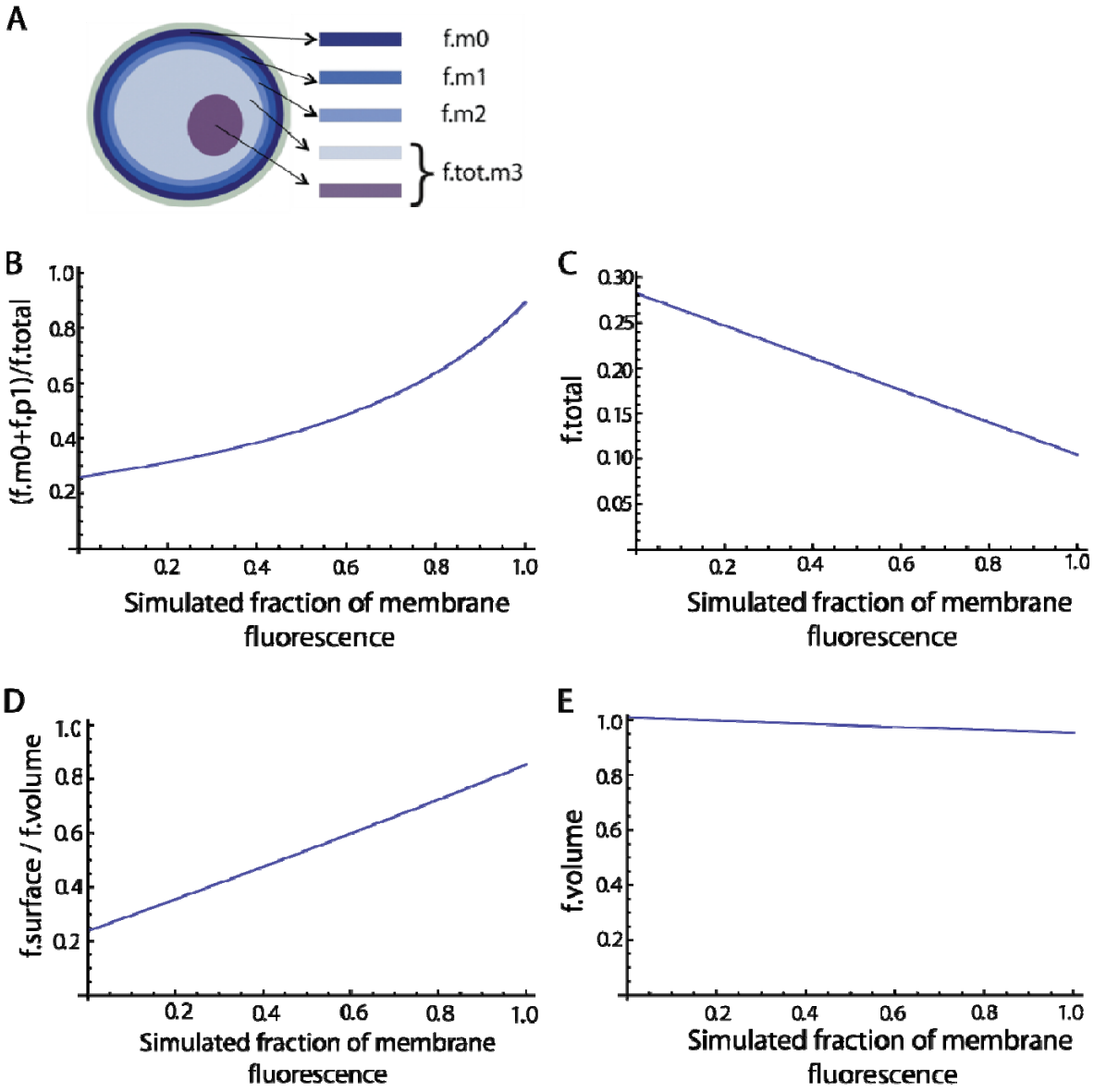

Figure S2: A) Schematic representation of subcellular regions defined by Cell-ID, described in Table S2. B) Candidate recruitment statistic ((f.m0+f.p1)/f.total) dependence on the simulated fraction of membrane fluorescence. C) dependence of f.total with the simulated fraction of membrane fluorescence. D)

Recruitment statistic (f.surface/f.volume) vs. simulated fraction of membrane fluorescence. E) Volume fluorescence (f.volume) vs. simulated recruitment.

To keep the simulation simple we did some rough approximations that don´t necessarily hold for real cells and microscopes. This is justified because the main objective of these simulations was to derive a general understanding of the functional dependence of Cell-ID´s variables with the fluorescence distribution, and not a quantitative relationship used as a calibration. In fact, we were able to corroborate experimentally many conclusions drawn from the simulations (Figure 2).

Using the simulation method described above we studied the usefulness of several candidate statistics calculating the simulated fraction of recruitment.

The first normalized statistic tested was the membrane fluorescence divided by the total fluorescence, both integrated in the focal plane. As a measure of membrane fluorescence we used the sum of f.m0 (the fluorescence at the cell´s boundary) and f.p1 (the fluorescence in an annular region one pixel wider than the boundary). This was done because a significant fraction of the membrane fluorescence reached the area associated with f.p1. The total fluorescence f.total is defined as

$$f.total = f.m0 + f.m1 + f.m2 + f.tot.m3 \qquad \text{Equation S3}$$

This candidate statistic has a non-linear relationship with the recruitment level (Figure S2B), caused by a decrease of the “total” fluorescence with the recruitment level (Figure S2C).

To obtain a measure of total fluorescence independent of the recruitment level, we calculated the volume fluorescence according to the following formula

$$\begin{aligned} f.volume = & \left(\frac{f.tot.m3}{a.tot.m3} - f.bg \right) \frac{4\pi}{3} \left(-3 + \frac{maj.axis + \min.axis}{4} \right)^3 \\ & + \left(\frac{f.m2}{a.m2} - f.bg \right) 4\pi \left(-2 + \frac{maj.axis + \min.axis}{4} \right)^2 \\ & + \left(\frac{f.m1}{a.m1} - f.bg \right) 4\pi \left(-1 + \frac{maj.axis + \min.axis}{4} \right)^2 \\ & + \left(\frac{f.m0}{a.m0} - f.bg \right) 4\pi \left(\frac{maj.axis + \min.axis}{4} \right)^2 \\ & + \left(\frac{f.p1}{a.p1} - f.bg \right) 4\pi \left(1 + \frac{maj.axis + \min.axis}{4} \right)^2 \end{aligned} \qquad \text{Equation S4}$$

The “surface fluorescence” was calculated as

$$f.surface = \left(\frac{f.m0}{a.m0} - f.bg \right) 4\pi \left(\frac{maj.axis + \min.axis}{4} \right)^2 + \left(\frac{f.p1}{a.p1} - f.bg \right) 4\pi \left(1 + \frac{maj.axis + \min.axis}{4} \right)^2$$

Equation S5

The recruitment statistic was calculated as the ratio of surface to volume fluorescence.

As can be seen in Figure S2E, the volume fluorescence is independent of the fluorescence distribution, thus resulting in a linear relationship between the recruitment statistic and the simulated fraction of membrane fluorescence (Figure S2D).

3. Correcting for changes in the focal plane

The cell boundary is determined by Cell-ID using a purposely defocused bright field image (4), and this boundary coincides with the periphery of the cell at the equatorial plane. Thus, if one acquires the fluorescence image focusing on the cell's equatorial plane, the boundary pixels correspond to the membrane. However, if the focus is above or below the equator of the cell, the section of the cell is smaller and thus the boundary found by Cell-ID does not coincide with the cell's membrane (see image montage in Figure S3). Consequently, if we were to use confocal images acquired at focal planes different from the cell's equatorial plane, we would be underestimating the true membrane recruitment level. Thus, the recruitment statistic strongly depends on the fine focus of the image (Figure S3).

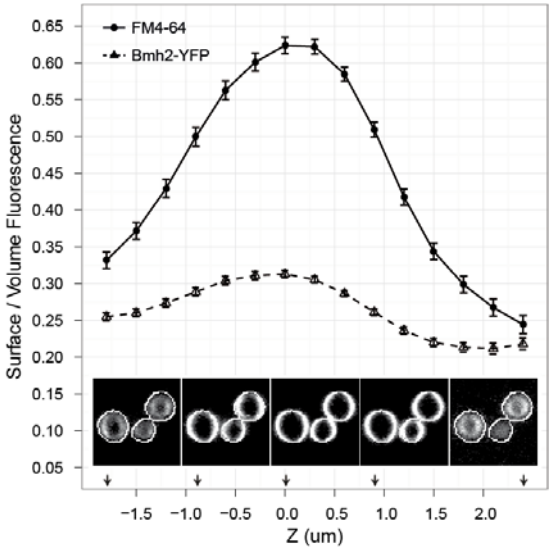

Figure S3: Recruitment statistic vs. focal plane for a membrane distribution (FM4-64, circles, solid line) or cytoplasmic distribution (Bmh2-YFP, triangles, dashed line) of fluorescence. The image montage shows the change of apparent fluorescence distribution with the focal plane for a cell stained with FM4-64. Arrows in the X axis indicate the focal plane of each image.

Small changes in the focal plane between different images are unavoidable, and even within the same image cells of different size have their equatorial planes at different heights. Moreover, changes in the focal plane do occur within a time course because of focus drift. The focus drift can be corrected by real-time focusing systems, but the two previous issues remain to be addressed.

To reduce this variability we modified the imaging protocol and acquired short Z stacks at each time point (5 to 7 slices, spaced by 0.4-0.5 μm). We then selected the "in-focus" image, determined as the image that maximizes the recruitment statistic for a particular Z stack (Figure S3). In this way the selection of the focal plane is independent of changes in the fine focus of each image and to focus drift. If single cell signal is strong enough, the focal plane can be determined independently for each cell.

4. Uncertainty estimation of membrane recruitment

The recruitment statistic depends strongly on the boundary determined by Cell-ID. In turn, this boundary is based on a black halo formed around cells in bright field images with the focal plane around 2μm below the equatorial plane of the cell. Because of small irregularities in the glass width, small inclinations of the plate and the fact that the height of the equatorial plane of a cell depends on its size, it is impossible to obtain exactly the same halo for all cells. This results in a small variability in how the cell boundary is found, relative to the plasma membrane of the cell. This variability can be ignored when measuring total fluorescence, but produces a significant variability in the basal level of the recruitment statistic.

Because we acquire time courses (following the same cells through time) we can measure the increase of the recruitment statistic after stimulation, thus eliminating the artifactual cell-to-cell variability mentioned above. One way to measure the increase in a statistic is to subtract the level before stimulation. Although very simple, this method implicitly and incorrectly assumes that the pre-stimulation level is measured without uncertainty, and is not well suited for the noisy data obtained in single cell measurements.

The approach used in this work was to subtract the "cell effect" to each data point. In the context of linear models, the value of a response variable Y of cell i at time j (Y_{ij}) can be interpreted as the sum of a population mean μ, a "cell effect" α_i, a "time effect" β_j, and an "interaction term" γ_{ij}, usually considered as the error in statistical techniques like repeated measures. Note that we do not include a "treatment effect" because this analysis is done independently for each treatment.

$$Y_{ij} = \mu + \alpha_i + \beta_j + \gamma_{ij}$$

Equation S6

The response variable (the recruitment statistic in our case) corrected by the "cell effect" is defined as

$$Y_{ij}^{*} = \mu + \beta_j + \gamma_{ij} = Y_{ij} - \alpha_i = Y_{ij} - \frac{1}{T}\sum_{j=1}^{T}(Y_{ij} - \mu)$$

Equation S7

where T is the total amount of time points measured. In Figure S4A and B we show example traces of single cells before (S4A) and after (S4B) applying this correction. The 95% confidence interval for the mean of the corrected response variable (Y^*_{ij}) was used as a measure of the uncertainty.

The uncertainty calculated in the described manner is typically around 10% of the maximal value, although it depends on the signal-to-noise ratio of the image, which in turn depends on the total fluorescence of the strain measured and the acquisition parameters used (laser intensity, exposure time, etc.).

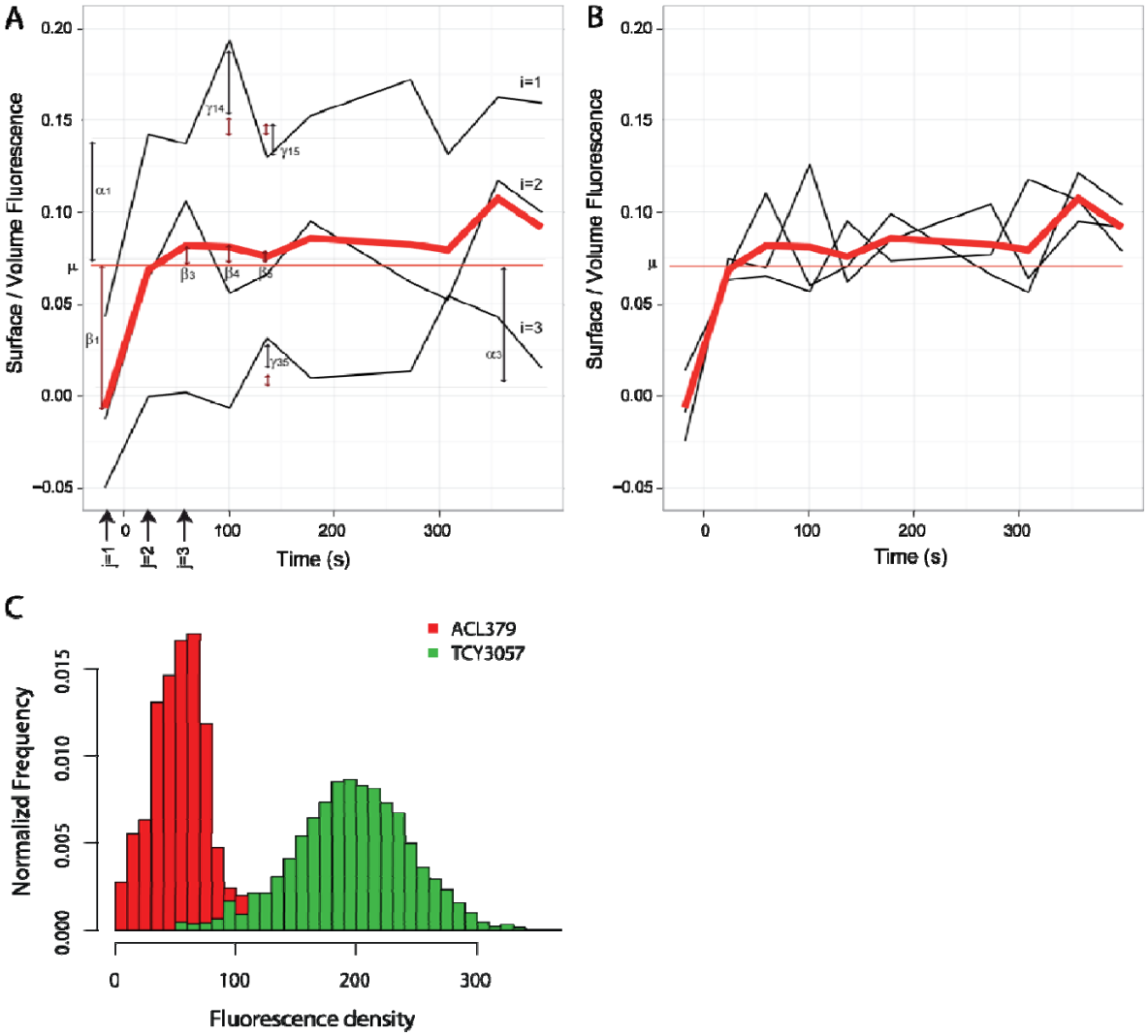

Figure S4: Recruitment statistic uncertainty estimation. A) The raw traces for three random cells are shown in black and the mean as a thick red line. Horizontal thin gray lines denote the mean of each cell, and the horizontal thin red line is the population average μ. Some coefficients of the linear model are annotated. B) Traces corrected by the "cell effect" (α_i) for the same cells. C) Distribution of fluorescence in the YFP channel for the YFP-Ste5 strain TCY3057, and its parental strain ACL379 with no fluorescent protein.

The calibrated recruitment level also depends on the estimation of the slope of the calibration curve ρ, and the fraction of autofluorescence f_{auto} (see equation 1, main text). The estimate for ρ is 0.291±0.016 (see Figure 2, main text) so the relative error of this coefficient is 5.5%.

The fraction of autofluorescence f_{auto} can be estimated comparing the distribution of fluorescence intensity of the YFP-Ste5 strains against the distribution of fluorescence of the parental strain with no fluorescent proteins (ACL379) in the YFP channel (Figure S4C). The wide distributions observed and the partial overlap in fluorescence levels between these two strains make the determination of the autofluorescence level at the single cell level very uncertain. A precise measure of autofluorescence can only be obtained at the population level. For TCY3057 (shown in Figure S4C) the fraction of autofluorescence is 0.27±0.02, but this value depends on the level of expression of YFP-Ste5, thus it was calculated for each strain independently.

Note than when comparing different data points of the same strain (as in Figure 3A), the uncertainty in the calibration is not relevant. This uncertainty is only important to calculate the absolute fraction of recruitment. To differentiate between these two sources of uncertainty, the confidence interval for the mean was plotted as an error bar of the data point and the uncertainty in the calibration as an error bar of the ticks in the y axis. When comparing the absolute recruitment level among strains (as in Figure 4), both uncertainty sources were added up and represented as error bars of the data points.

5. Ste5 membrane recruitment controls

Autofluorescence distribution does not change with pheromone stimulation

As mentioned in the main text, we assume that the autofluorescence does not change its subcellular distribution upon pheromone stimulation. To test this assumption we measured membrane recruitment in ACL379 cells, the parental strain with no fluorescent protein (Figure S5 A). It can be observed that the recruitment statistic for ACL379 has the same behavior with or without 1μM α-factor, within the experimental uncertainty. Note that the signal to noise ratio is very low in this strain, and thus the curves are very noisy. For comparison, traces of strain TCY3056 (ste5::YFP-STE5, Table S1) with and without α-factor are included (Figure S5 A).

Basal recruitment of Ste5 is negligible

Because of the high variability of the basal level of the recruitment statistic, we measured the increase upon pheromone stimulation. This implicitly assumes that the basal recruitment (i.e. the basal fraction of membrane bound Ste5) is negligible. To test this assumption we compared the levels of the recruitment statistic in a WT strain (TCY3127) with a Δ*ste4* strain (TCY3205), both harboring two integrations of the P_{STE5}-YFP-STE5 construct (Table S1), in the absence of stimulation. We observed no significant difference between strains (Figure S5B, p-value=0.78), confirming that basal recruitment is negligible.

Membrane recruitment of Ste5 depends on Ste4

We also compared the membrane recruitment in these strains (Figure S5C) after pheromone stimulation. No membrane recruitment of Ste5 could be detected in the Δ*ste4* strain, confirming that plasma membrane recruitment of Ste5 is Ste4 dependent, as previously reported (6).

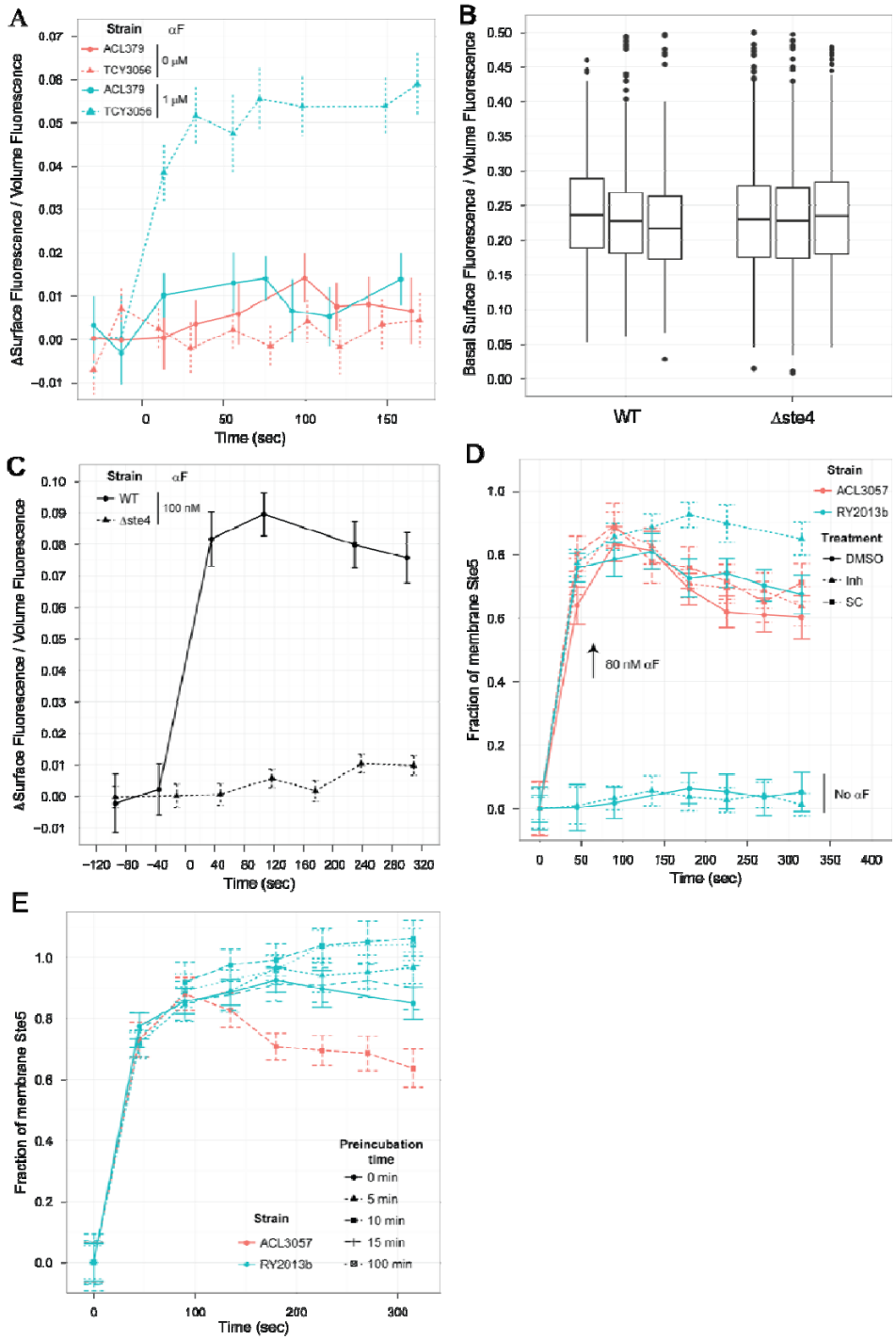

Figure S5. A) Increase in the recruitment statistic upon stimulation with saturating α-factor (blue curves) or SC medium (red curves), of strain TCY3056 (triangles, dashed line) or its parental strain with no fluorescent proteins ACL379 (circles, solid line). B: Basal level of the recruitment statistic for WT (TCY3127) or ⊗ste4 (TCY3205) strains. Three images for each strain were quantified. The thick line represents the median, and the box spans the interquartile range (iqr). Whiskers extend to the last data point within 1.5 times the iqr away from the box. Points represent cells outside this range. There is no significant difference among strains (p-value=0.78, ANOVA). C) Increase in the recruitment statistic upon stimulation with 100 nM α-factor of the WT strain (circles, solid line) or the Δ*ste4* strain (triangles, dashed line). D)Increase in Ste5 membrane recruitment in strain ACL3057 (wt FUS3, red curves) and strain RY2013b (FUS3-Q88A, blue curves), with (triangles) or without (squares) 10 µM of the inhibitor 1-NM-PP1. The effect of the carrier (0.1% DMSO) was tested on strain ACL3057 (circles and solid red line). The effect of the inhibitor in unstimulated cells (No αF) was tested in strain RY2013b. E) Ste5 recruitment dynamics in cells preincubated different times with 10 µM of 1-NM-PP1. In the 0 min curve, the inhibitor was added with the pheromone.

Inhibitor 1-NM-PP1 only affects Ste5 recruitment in FUS3-Q93A strains

Neither the inhibitor 1-NM-PP1 at a concentration of 10 µM, nor the solvent by iteself (DMSO 0.1%) affected recruitment of Ste5 in cells with wt Fus3 (Figure S5D, red curves). The strain with the sensitive allele FUS3-Q93A (RY2013b) has normal Ste5 membrane recruitment in the absence of the inhibitor (Figure S5D, top blue curves). The inhibitor alone (with no αF) produces no response at the level of Ste5 membrane recruitment within the first 5 minutes of treatment (Figure S5D, bottom blue curves). Ten minutes of preincubation with the inhibitor results in complete elimination of the decline phase in membrane recruitment of Ste5 (Figure S5E).

6. Bimolecular association model

As explained in the main text, we implemented the simple bimolecular association model shown below.

$$Ste5 + G \underset{k_{off}}{\overset{k_{on}}{\rightleftharpoons}} Ste5 \cdot G$$

Equation S8

Here k_{on} and k_{off} are the binding and unbinding rates, respectively. Writing ODEs using mass action rate laws and considering the conservation of total Ste5 ($Ste5_{tot}$=Ste5+Ste5.G) and total binding sites (G_{tot}=G+Ste5.G), the system can be simplified to a single differential equation

$$\frac{d\,Ste5 \cdot G}{dt} = k_{on} \frac{\left(Ste5_{tot} - Ste5 \cdot G\right)}{V_c} \frac{\left(G_{tot} - Ste5 \cdot G\right)}{V_m} - k_{off} \frac{Ste5 \cdot G}{V_m}$$

Equation S9

Note that the variables Ste5.G, $Ste5_{tot}$ and G_{tot} represent number of molecules and not concentration. V_c is the cytosol volume through which Ste5 can diffuse, estimated as V_c=36.4 fl (7). V_m represents the volume of a layer adjacent to the membrane to which Ste5 is confined when

recruited (8). It is not necessary to estimate the value of V_m as it cancels out in the steady state solution of the model

$$Ste5 \cdot G_{eq} = \frac{1}{2}\left(Kd\ V_c + G_{tot} + Ste5_{tot} - \sqrt{\left(Kd\ V_c + G_{tot} + Ste5_{tot}\right)^2 - 4G_{tot}\ Ste5_{tot}}\right)$$ Equation S10

where $Kd=k_{off}/k_{on}$. This model was fitted to the experimental dataset for membrane bound Ste5 at peak recruitment and time points thereafter. Note the model has only two parameters to be fitted, G_{tot} and the product $Kd \times V_c$. $Ste5_{tot}$ was defined by the number of integrations of the P_{STE5}-YFP-STE5 construct of each strain.

Fitting the model to the data using non-linear least squares or minimizing the χ^2 statistic ($\chi^2=\Sigma((Y_i-\mu_i)/\sigma_i)^2$) rendered equivalent results. Using the χ^2 statistic has the advantage that the value can be compared with the critical value of a χ^2 distribution of the corresponding degrees of freedom, and a region of "acceptable parameters" can be defined (9)(Figure 4D-F). When the parameters ($Kd \times V_c$, G_{tot}) are in this region, the data does not reject the model at $\alpha=0.05$.

7. Dependence of CFP-Ste4 levels with the number of YFP-Ste5 integrations

The bimolecular association model assumes that the number of binding sites is the same in the strains with different number of integrations of the P_{STE5}-YFP-STE5 construct. To verify this assumption we integrated a variable number of the P_{STE5}-YFP-STE5 construct in strain TCY3099 (ste5::YFP-STE5, CFP-STE4). Therefore, we created a series of strains with different amounts of YFP-STE5, but a single copy of CFP-STE4 replacing the STE4 ORF.

We quantified CFP fluorescence at the cell membrane of these strains by epi-fluorescence microscopy, using Cell-ID (variables f.p1+f.m0+f.m1+f.m2 corrected by background fluorescence). Because CFP fluorescence was very dim and single cell data was not reliable, we averaged all cells of each image, and acquired 9 images per strain (three images per well, three wells per strain).

Statistical analysis of this data reveled that there is a significant decrease of CFP-STE4 in TCY3099 (CFP-STE4, P_{STE5}-YFP-STE5 x1) as compared to the strain TCY3100 (CFP-STE4, WT, untagged STE5), or the strain YAB3771 (CFP-STE4, P_{STE5}-YFP-STE5 x2). Because of this decrease, this strain was not included in further analysis. Note that YAB3771 is a derivative of TCY3099, indicating that the reduction in CFP-STE4 level introduced when replacing the WT STE5 by the YFP-STE5, was rescued by an increase in the dose of YFP-STE5. Further increase in the dose of YFP-STE5 produced a small increase in CFP-STE4 level that saturated at four integrations (Figure 4C).

8. Diffusion time for Ste5

Membrane recruitment of Ste5 involves diffusion through the cytosol and a binding reaction to a membrane associated binding site. To investigate if the overall rate of recruitment was limited by the binding reaction rate (reaction limited) of by the rate of diffusion (diffusion limited), we decided to calculate the characteristic time for diffusion from the cytosol to the plasma membrane. If this time is similar to the measured recruitment time (~40 sec) the reaction is diffusion limited. On the other hand if the calculated diffusion time is much smaller than the measured dynamic of Ste5 membrane recruitment, recruitment is reaction limited.

For simplicity we will assume a spherical cell, of radius R_{cell}, with a homogeneous initial distribution of Ste5. Because we are interested in the diffusion time we assume a perfectly absorbing membrane, i.e. the boundary condition is Ste5=0 at $r=R_{cell}$. Note that here Ste5 refers to the "free", diffusible Ste5 and not the membrane bound Ste5. The diffusion equation in spherical coordinates is

$$\frac{1}{r^2}\frac{\partial}{\partial r}\left(r^2\frac{\partial}{\partial r}[Ste5](r,t)\right)=\frac{1}{D}\frac{\partial}{\partial t}[Ste5](r,t) \qquad \text{Equation S11}$$

where D is the diffusion constant, [Ste5](r,t) is the cytoplasmic concentration of Ste5 at time t and a distance r from the cell´s center. This equation is equivalent to the heat diffusion in a sphere with a constant temperature at its boundary, and can be solved in close form (10). The solution for Ste5(t), the total amount of cytoplasmic Ste5 in the cell, is given by

$$Ste5(t)=Ste5(0)\sum_{n=1}^{\infty}A_n\exp\left(-\frac{t}{\tau_n}\right)$$
$$A_n=\frac{6}{(n\pi)^2} \qquad \text{Equation S12}$$
$$\tau_n=\frac{1}{D}\left(\frac{R_{cell}}{n\pi}\right)^2$$

where Ste5(0) is the total amount of cytoplasmic Ste5 at time zero. The dynamic of Ste5 is dominated by the first term of the series with characteristic time $\tau_1=R_{cell}^2/(\pi^2 D)$.

We estimated the diffusion constant for Ste5 from the FCS data from Slaughter et al. 2007 (11), which results in D = 6.6 ± 0.3 $\mu m^2 s^{-1}$, and used R_{cell}=2.4±0.2μm. Using this values the characteristic time of diffusion (i.e. the time it takes for 63% of the total Ste5 to diffuse to the membrane) results in τ = 0.09 ± 0.01s. The same value was obtained doing numerical simulations with Virtual Cell (12).

It takes around a minute for Ste5 to recruit from the cytoplasm to the membrane upon pheromone stimulation (Figure 2, main text), that is ~1000 times slower than the calculated time for diffusion, therefore membrane recruitment of Ste5 is reaction limited.

9. Supporting References

1. Colman-Lerner, A., A. Gordon, E. Serra, T. Chin, O. Resnekov, D. Endy, C. G. Pesce, and R. Brent. 2005. Regulated cell-to-cell variation in a cell-fate decision system. Nature 437:699-706.
2. Gordon, A., A. Colman-Lerner, T. E. Chin, K. R. Benjamin, R. C. Yu, and R. Brent. 2007. Single-cell quantification of molecules and rates using open-source microscope-based cytometry. Nat Methods 4:175-181.
3. Yu, R. C., C. G. Pesce, A. Colman-Lerner, L. Lok, D. Pincus, E. Serra, M. Holl, K. Benjamin, A. Gordon, and R. Brent. 2008. Negative feedback that improves information transmission in yeast signalling. Nature 456:755-761.
4. Bush, A., A. Chernomoretz, R. Yu, A. Gordon, and A. Colman-Lerner. 2012. Using Cell-ID 1.4 with R for Microscope-Based Cytometry. Curr Protoc Mol Biol Chapter 14:Unit14 18.
5. Zhang, B., J. Zerubia, and J. C. Olivo-Marin. 2007. Gaussian approximations of fluorescence microscope point-spread function models. Appl Opt 46:1819-1829.
6. Pryciak, P. M., and F. A. Huntress. 1998. Membrane recruitment of the kinase cascade scaffold protein Ste5 by the Gbetagamma complex underlies activation of the yeast pheromone response pathway. Genes Dev 12:2684-2697.
7. Uchida, M., Y. Sun, G. McDermott, C. Knoechel, M. A. Le Gros, D. Parkinson, D. G. Drubin, and C. A. Larabell. 2011. Quantitative analysis of yeast internal architecture using soft X-ray tomography. Yeast 28:227-236.
8. Kholodenko, B. N., J. B. Hoek, and H. V. Westerhoff. 2000. Why cytoplasmic signalling proteins should be recruited to cell membranes. Trends Cell Biol 10:173-178.
9. Raue, A., C. Kreutz, T. Maiwald, J. Bachmann, M. Schilling, U. Klingmuller, and J. Timmer. 2009. Structural and practical identifiability analysis of partially observed dynamical models by exploiting the profile likelihood. Bioinformatics 25:1923-1929.
10. Ozisik, M. N. 1993. Heat Conduction. John Wiley & Sons, Inc.
11. Slaughter, B. D., J. W. Schwartz, and R. Li. 2007. Mapping dynamic protein interactions in MAP kinase signaling using live-cell fluorescence fluctuation spectroscopy and imaging. Proc Natl Acad Sci U S A 104:20320-20325.
12. Loew, L. M. 2002. The Virtual Cell project. Novartis Foundation symposium 247:151-160; discussion 160-151, 198-206, 244-152.